IOPscience iopscience.iop.org

Home Search Collections Journals About Contact us My IOPscience

Radiofrequency multielectrode catheter ablation in the atrium

This content has been downloaded from IOPscience. Please scroll down to see the full text.

1999 Phys. Med. Biol. 44 899

(http://iopscience.iop.org/0031-9155/44/4/007)

View the table of contents for this issue, or go to the journal homepage for more

Download details:

IP Address: 128.4.147.111
This content was downloaded on 04/02/2014 at 18:16

Please note that terms and conditions apply.

Phys. Med. Biol. **44** (1999) 899–915. Printed in the UK PII: S0031-9155(99)99724-5

Radiofrequency multielectrode catheter ablation in the atrium

Dorin Panescu†, Sidney D Fleischman†, James G Whayne†,
David K Swanson†, Mark S Mirotznik‡, Ian McRury§ and David E Haines§

† Boston Scientific, 2710 Orchard Parkway, San Jose, CA 95134, USA
‡ The Catholic University of America, Department of Electrical Engineering, Pangborn Hall, Washington DC 20064, USA
§ The University of Virginia, Health Science Center, Charlottesville, VA 22908, USA

Received 30 November 1998

Abstract. We developed a temperature-controlled radiofrequency (RF) system which can ablate by delivering energy to up to six 12.5 mm long coil electrodes simultaneously. Temperature feedback was obtained from temperature sensors placed at each end of coil electrodes, in diametrically opposite positions. The coil electrodes were connected in parallel, via a set of electronic switches, to a 150 W 500 kHz temperature-controlled RF generator. Temperatures measured at all user-selected coil electrodes were processed by a microcontroller which sent the maximum value to the temperature input of the generator. The generator adjusted the delivered power to regulate the temperature at its input within a 5 °C interval about a user-defined set point. The microcontroller also activated the corresponding electronic switches so that temperatures at all selected electrodes were controlled within a 5 °C interval with respect to each other. Physical aspects of tissue heating were first analysed using finite element models and current density measurements. Results from these analyses also constituted design input. The performance of this system was studied *in vitro* and *in vivo*.

In vitro, at set temperatures of 70 °C, 85% of the lesions were contiguous. All lesions created at set temperatures of 80 and 90 °C were contiguous. The lesion length increased almost linearly with the number of electrodes. Power requirements to reach a set temperature were larger as more electrodes were driven by the generator. The system impedance decreased as more electrodes were connected in the ablation circuit and reached a low of 45.5 Ω with five coil electrodes in the circuit.

In vivo, right atrial lesions were created in eight mongrel canines. The power needed to reach 70 °C set temperature varied between 15 and 114 W. The system impedance was 105 ± 16 Ω, with one coil electrode in the circuit, and dropped to 75 ± 12 Ω when two coil electrodes were simultaneously powered. The length and the width of the lesion set varied between 17.6 ± 6.1 and 59.2 ± 11.7 mm and 5.9 ± 0.7 and 7.1 ± 1.2 mm respectively. No sudden impedance rises occurred and 75% of the lesions were contiguous. From the set of contiguous lesions, 90% were potentially therapeutic as they were transmural and extended over the entire target region. The average total procedure and fluoroscopy times were 83.4 and 5.9 min respectively. We concluded that the system can safely perform long and contiguous lesions in canine right atria.

1. Introduction

Atrial fibrillation (Afib) is a common clinical problem which affects more than 2 million people in the USA alone. One study reports 0.4% worldwide prevalence of Afib, with a high of ≈1% in the USA (Cox *et al* 1991a). People older than 60 years are most affected, 10.2% of them suffering from Afib. Patients with Afib experience unpleasant irregular heartbeats, impaired haemodynamics caused by loss of atrioventricular synchrony and vulnerability to thromboembolic complications (Cox *et al* 1991b). Atrial fibrillation is also associated with a 4–6% yearly incidence of strokes and is linked with a twofold

0031-9155/99/040899+17$19.50 © 1999 IOP Publishing Ltd

increase in cardiovascular mortality (Wolf *et al* 1991). An ideal treatment for Afib would have three positive consequences: (1) restore a regular ventricular rhythm, (2) normalize cardiac haemodynamics and (3) alleviate the vulnerability to thromboembolism. At the present time, Afib therapy is most commonly attempted by medication. The numerous follow-ups, high management cost and disturbing side effects of the drug therapy have made the medical community search for more effective solutions (Cox *et al* 1991a, Roberts *et al* 1993). It has been reported that patients had a regular ventricular rhythm restored, the cardiac haemodynamics normalized and the vulnerability to thromboembolism decreased after being treated with the surgical procedure called the 'maze'. In order to stop the propagation of fibrillating wavefronts, the 'maze' procedure employs open-heart linear surgical incisions at predetermined locations in both right and left atria (Cox *et al* 1991a, b). Since this procedure requires open-chest surgery, other less invasive treatments are currently under investigation.

Radiofrequency catheter ablation is a technique whereby currents with frequencies between 300 kHz and 1 MHz are applied through electrodes to tissue. Tissue in the immediate vicinity of the electrode is heated by the Joule effect, whereas farther away its temperature is increased mainly by thermal conduction. The myocardial region heated above $\approx 50\,^{\circ}\mathrm{C}$ becomes non-viable and defines the lesion volume. Fundamentals of the RF ablation technique have been presented elsewhere (Cosman and Rittman 1995, Nath *et al* 1993, Panescu *et al* 1995a, Panescu 1997). Swartz *et al* (1994) reported that replicating the 'maze' by RF catheter ablation may cure Afib in humans. Using a 'drag and burn' technique with a 4 mm standard ablation electrode, they created RF lesions in both atria. Swartz *et al* (1994) indicated that contiguous and transmural atrial RF lesions have increased chances of successful therapeutic outcome. Consequently, systems optimized for atrial RF ablation procedures should have the ability to generate long (for example >4 cm) and contiguous lesions.

We present current densities and thermal profiles generated by long multielectrode structures, mechanical features of a steerable catheter and performance of a multielectrode multitemperature-sensor temperature controller. Results from *in vivo* atrial RF ablations conclude our study.

2. Methods and apparatus

The multielectrode catheter (MEC) analysed by this study has the structure shown in figure 1. The MEC has bidirectional steering and carried up to six 7F 12.5 mm long stainless steel coil electrodes (1F $\approx$ 0.33 mm). The interelectrode distance was 2 mm. The system has the capability of delivering RF power simultaneously to any user-selected combination of coils, from any one coil to up to all six coils. Unipolar electrograms were available from the distal sensing electrode and from any of the coil electrodes. Bipolar electrograms were available from any bipolar pair of electrodes, such as the distal electrode and the first coil electrode or any combination of two adjacent coil electrodes. Pacing could be performed from the distal electrode or from any of the coil electrodes.

2.1. Specific absorption rates and current densities of electric fields generated by the multielectrode structure

The determination of optimal temperature-sensor placement has to consider information resulting from current density and temperature distributions. This section describes the methods used to measure the current density profiles generated by the MEC. The change in temperature (T) during ablation at any point in the body is given by the heat transfer equation

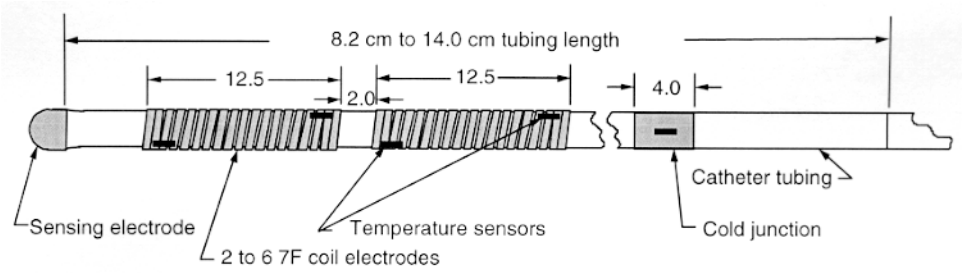

Figure 1. The multielectrode catheter carries up to six 7F 12.5 mm long coil electrodes spaced 2 mm apart. A distal sensing electrode is used to record electrograms. The proximal ring is used as a cold junction for the thermocouples associated with the coil electrodes.

(Shitzer and Eberhart 1985):

$$\rho c \frac{\partial T}{\partial r} = \nabla \cdot k \nabla T + \boldsymbol{J}\boldsymbol{E} - h_{\mathrm{bl}}(T - T_{\mathrm{bl}}) - Q_{\mathrm{el}} \qquad h_{\mathrm{bl}} = \rho_{\mathrm{bl}} c_{\mathrm{bl}} w_{\mathrm{bl}} \tag{1}$$

where ρ is density, c is specific heat capacity, k is thermal conductivity, $\boldsymbol{J}$ is current density, $\boldsymbol{E}$ is intensity of the electric field, ρ_{bl} is the blood density, c_{bl} is the blood heat capacity, w_{bl} is the blood perfusion, T_{bl} is the blood temperature and Q_{el} accounts for the heat exchanged between the tissue and the ablation electrode and usually is negligible.

The specific absorption rate (SAR) is defined as (Mirotznik *et al* 1996)

$$\mathrm{SAR} = (1/\rho)\boldsymbol{J}\boldsymbol{E} \tag{2}$$

measured in W kg^{-1} and is an important parameter in defining the tissue-temperature profiles. The scalar current density J can be computed from the SAR values as

$$J = \sqrt{\sigma \rho \mathrm{SAR}} \tag{3}$$

where σ is electrical conductivity. The current density values provide information about the potential location of high-temperature tissue regions. We have shown in a previous study that the SAR can be computed by measuring T at times t_1 and t_2, during the beginning of the transient phase of the RF application (Panescu *et al* 1995a):

$$\mathrm{SAR} = c \frac{T(t_2) - T(t_1)}{t_2 - t_1}. \tag{4}$$

The temperature values needed to compute the SAR based on (4) were measured along an MEC introduced in a tank of flowless saline. The standard IEEE C95.3-1991 (IEEE 1992) recommends SAR measurements be taken in tissue-equivalent media. The current density distribution, thus the SAR, is affected by the electrical resistivity of the medium. To meet this requirement, the concentration of saline was chosen to be equal to 0.15%, matching the average cardiac tissue resistivity of ≈450 Ω cm. The density, heat capacity and thermal conductivity of the 0.15% saline also represent a reasonable approximation of the corresponding cardiac tissue values shown in table 1 (Rabbat 1990, Incropera and DeWitt 1985, ASM 1992). The temperature values in (4) were acquired at a sampling frequency of 100 Hz with a 0.25 mm thermistor having a thermal response of less than 0.1 s. The thermistor leads were twisted, shielded and aligned perpendicular to the electric field lines so that the RF interference was minimal (Mirotznik *et al* 1996). The temperature probe was calibrated at slowly (≈1–2 min) increasing and decreasing temperatures: the saline bath was warmed to 35 °C in about 1 min and then allowed to cool freely to 22 °C during which readings were taken with both the SAR probe and a standard Vitek temperature probe. The probes were placed in close proximity of

less than 1 mm. No hysteresis was found and the errors were confined within $\pm 0.1\,^{\circ}$C. We verified the apparatus for any possible coupling between the RF source and the SAR probe: the RF source was turned on–off a series of times while the SAR probe was kept at 1 cm distance from the MEC electrode surface. Maximum equivalent temperature interference less than $0.05\,^{\circ}$C was measured.

To measure temperature with acceptable spatial resolution, the SAR thermistor was mounted on a three-axis stage controlled by stepping motors. Using this apparatus we were able to locate the SAR probe with a spatial resolution of 0.5 mm. Temperature readings were taken along the coil electrodes shown in figure 1 with a step size of 1 mm at six depths from their surface: 0, -1, -2, -3, -4 and -5 mm. Two sets of SAR measurements were performed. During the first set of measurements, 20 W of RF power (500 kHz) were applied between a single coil electrode and a 144 cm^2 patch electrode. Five different coils of the MEC were tested in the saline tank. At each of the six depths, 24 measurements were taken by moving the probe parallel to the coil in 1 mm steps, starting 5 mm away from the proximal end of each tested coil. During the second set of measurements, 20 W of RF power were simultaneously applied to two adjacent coil electrodes. Five different two-coil groups were tested. At each of the six depths, 38 measurements were taken by moving the probe parallel to the coils in 1 mm steps, starting 5 mm away from the proximal end of the proximal coil. In each case, the initial temperature of the bath was measured at $22\,^{\circ}$C, the RF power was turned on for 0.5 s, $t_1 = 0.1$ s, and $t_2 = 0.35$ s. Within this time interval, the temperature measured by the probe increased by about $0.5\,^{\circ}$C to about $10\,^{\circ}$C. Because the saline was not circulated inside the tank, and given the short duration of the temperature measurement, the convection effects were negligible. The exact magnitude of the temperature variation depended on the physical location of the probe with respect to coils. After the saline returned to $T_0 = 22\,^{\circ}$C, the thermistor was moved to a new location and the measurements were continued until the region of interest was completely mapped. Using (3), the SAR maps were converted to current density profiles.

2.2. Finite element modelling of temperature distributions generated by a coil electrode

The search for optimal MEC temperature-sensor placement was also based on information about tissue-temperature profiles. We employed the finite element (FE) method to numerically approximate the solution to (1). The current density and the electric field intensity can be computed from the Laplace equation:

$$\nabla \cdot \sigma \nabla V = 0 \tag{5}$$

and the equation $\boldsymbol{J} = \sigma \boldsymbol{E} = -\sigma \nabla V$, where σ is electrical conductivity and V is potential. Equations (1) and (5) apply to all regions of the tissue–electrode–blood system. Tong and Rossettos (1977) have presented details regarding the FE method. In this study we used mixed boundary conditions for the electrical model and Dirichlet boundary conditions for the thermal model. The current density was specified at the coil electrodes and the voltage was set to zero at the peripheral nodes of the model. The temperature was set to $37\,^{\circ}$C at the peripheral nodes. Because at 500 kHz, a frequency commonly used for ablation, tissue has mostly a resistive character (Rabbat 1990), we solved (5) only for the steady state using the root-mean-square values of voltage and current density as boundary conditions. The electrical model was considered linear. The thermal constants of tissue were of the order of several seconds. Therefore, we studied the transient solution to (1). We solved both (1) and (5) using COSMOS on an HP 715 workstation with a 75 MHz processor, 48 MB of main memory and 1 GB of hard-disk space. The ESTAR and HSTAR modules of COSMOS allowed us to perform coupled thermal–electrical transient analyses.

For these analyses, we used a 3D FE model of a 7F 12.5 mm coil electrode. The material of the coil electrode had a rectangular cross section, a width of 0.5 mm and thickness of 0.1 mm. The coil electrode had 19 windings spaced 0.17 mm apart. The electrode metal was modelled as stainless steel and the catheter body as an insulator. The ends of the coil electrode were covered by a 0.15 mm thin electrically and thermally insulating layer of ultraviolet-light-cured (UV) adhesive. Consequently, this layer was modelled as a region of very low electrical and thermal conductivities. The FE model simulated the coil electrode lying on a 4 cm thick slice of cardiac tissue. The coil electrode was modelled as being 50% of its diameter embedded into tissue and 50% exposed to blood. The region modelling the blood extended 4 cm above the cardiac tissue. The simulated blood–electrode–tissue region was 4 cm long. The overall FE model was formed of 9029 nodes and used 9056 hexahedral elements distributed on a non-uniform mesh. The FE mesh had high node density within the space extending 0.5 mm from the coil surface. For example, the space 0.5 mm beneath each coil winding was modelled using three-node longitudinal and radial FE nodal densities. The same FE nodal density was used to model the corresponding space beneath the intercoil gaps. The FE nodal density was reduced for regions extending beyond 5 mm around the coil electrode. The complexity of the FE model represented a trade-off between the total processing time and the numerical accuracy. Larger models required significantly longer processing time without significant improvements in accuracy. Table 1 presents the material properties of the FE regions included in this model (Rabbat 1990, Incropera and DeWitt 1985, ASM 1992). To estimate the effects of convective heat losses, a convective boundary coefficient was input into the FE solver. This coefficient was proportional to h_{bl} of equation (1), which was equal to 4×10^{-5} J mm^{-3} s^{-1} K^{-1} at the electrode–blood interface (Panescu 1997). To simulate the current distribution at the welded junction between the coil electrode and the wire connected to the RF source, current density boundary conditions were assigned at nodes distributed on a circle at the electrode central region. The total injected current was set at 0.42 A and generated a total RF power of $\approx$16 W. We found this level of power appropriate for reaching a maximum tissue temperature of $\approx$82 °C. During actual ablations, it is important to control the temperature below 100 °C in order to avoid tissue damage or blood coagulation due to overheating. The voltage was set to 0 V and the temperature to 37 °C on the external boundary of the model. The initial temperature at all nodes was set to 37 °C, assuming thermal equilibrium. To determine temperature distributions, coupled thermal–electrical 120 s transient FE analyses were performed at step sizes of 1.2 s. It is important to understand that FE simulations have limitations and have been shown to be accurate only within $\pm$10% to $\pm$20%, depending on the studied parameter (Panescu *et al* 1995a).

Table 1. Thermal and electrical properties of the finite element regions.

FE region	Material	ρ (g mm^{-3})	c (J g^{-1} K^{-1})	k (W mm^{-1} K^{-1})	σ (S mm^{-1})
Electrode	Stainless steel	8×10^{-3}	4.8×10^{-1}	1.5×10^{-2}	7.4×10^{3}
Tissue	Cardiac muscle	1.2×10^{-3}	3.2	5.5×10^{-4}	2.22×10^{-4}
Blood	Blood	10^{-3}	4.18	5.43×10^{-4}	6.67×10^{-4}
Catheter body	Polyurethane	7×10^{-5}	1.045	2.6×10^{-5}	10^{-8}
Coating	UV adhesive	3.2×10^{-5}	8.35×10^{-1}	3.8×10^{-5}	10^{-8}

2.3. The ablation system

Figure 2 shows a block diagram of the ablation system. The main blocks are: (1) an MEC, with its coil electrodes and associated temperature sensors, and a return 144 cm^2 pad electrode (GND

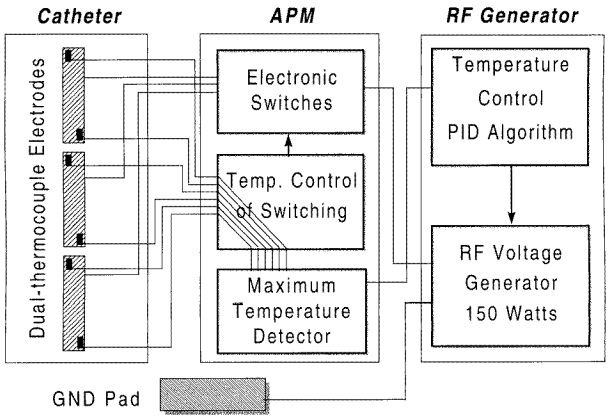

Figure 2. Block diagram of the ablation system. The APM monitors the temperatures at all sensors associated with the user-selected coil electrodes. The maximum temperature value is transmitted to the RF generator which controls the delivered power such that this value varies about a user-defined set point. The electronic power switches are controlled by the APM to regulate temperatures at all coils within a 5 °C interval.

pad); (2) an automated power-distribution module (APM) comprising a temperature monitoring unit, a microcontroller and electronic power switches which conducted or interrupted the parallel delivery of RF to the coil electrodes; and (3) a temperature-controlled RF generator, which regulated the level of RF power delivered to the APM based upon an input temperature value and a user-defined temperature set point. Thus, the electric current flows from one lead of the RF generator to one or more coils (via electronic switches) through tissue to the return electrode and back to the second lead of the RF generator. The user can select the coil electrodes to be used for RF energy delivery. As shown in figure 1, the MEC carried one temperature sensor at each edge of each of the coil electrodes. The sensors made good thermal contact with the coil electrodes. In this particular realization of the MEC, we used 0.1 mm Cu–Ct thermocouples (T type) to sense temperature. Thermistors could have been used with equal performance. We opted for thermocouples due to their smaller volumes. One Cu–Ct thermocouple was used to create the reference (cold) junction for all thermocouples carried by the coil electrodes. The cold junction thermocouple was attached in good thermal contact to a proximal Pt–Ir ring. During actual use, this ring sits in the blood pool. Thus, under normal conditions, the cold junction temperature is $\approx 37\,^{\circ}$C, the typical blood temperature. All other temperatures are read with respect to this reference temperature. To minimize RF interference in the temperature monitoring circuit, all thermocouples were electrically insulated from the coil electrodes and the cold junction ring, and had their leads twisted and passed through a metallic shield. The coil electrodes, the return electrode and the temperature sensors were connected to the APM. As mentioned above, each coil electrode was formed of 19 windings, spaced 0.17 mm apart, and had cross-sectional dimensions of 0.5×0.1 mm. Coils with smaller cross sections have been tested and did not provide enough heating due to higher equivalent electrical resistance. Coils with increased area had higher rigidity and thus negatively affected the MEC steerability. The interwinding spacing was selected based on measurements of the achievable curvature and angle of deflection between adjacent coils. Smaller curvatures improve steering capabilities. Lower values of the coil-to-coil deflection angle ensure a smooth profile of the MEC, thereby eliminating the formation of corners at intercoil gaps. Such corners can produce undesirable mechanical trauma to the endocardial surface and negatively affect the electrode–tissue contact.

The temperature monitoring unit of the APM read all temperature inputs corresponding to the user-selected coil electrodes (a total of twice the number of selected coil electrodes). Each selected coil electrode was assigned a temperature value (T_{CE}) equal to the higher of the two temperature readings obtained from the two thermocouples it carried. The coil electrodes were connected via a set of electronic switches to a 150 W 500 kHz generator. All selected T_{CE} values were processed by the APM's microcontroller which sent the maximum T_{CE} value to the temperature-monitoring input of the RF generator. The microcontroller also commanded on or off the corresponding electronic switches so that all T_{CE}s were contained within a 5 °C interval with respect to each other. The RF generator adjusted the delivered voltage such that the input temperature (i.e. maximum of T_{CE} values) varied about a user-defined set point. The RF generator also measured the system impedance between the coil electrodes and the return electrode. To avoid tissue damage due to overheating, the ablation system shut down when the system impedance was higher than 300 Ω.

2.4. In vitro method

Figure 3 illustrates the apparatus used to analyse the performance of the ablation system *in vitro*. The MEC was placed in good electrical contact with a 4 cm thick slice of bovine heart. The tissue laid over a 144 cm^2 rectangular return electrode. Using a holding fixture employing a force gauge, a constant force of 20 g was applied to the MEC shaft. Saline was circulated to all electrodes using a peristaltic pump connected to a 10 mm diameter hose with a multiple outlet terminal. The pump flow was 520 ml min^{-1}, yielding a local saline velocity of ≈12 cm s^{-1}. Considering an average aortic cross section of 7 cm^2, at this average velocity, the equivalent cardiac output would have been ≈5 l min^{-1}. In order to approximate the effects

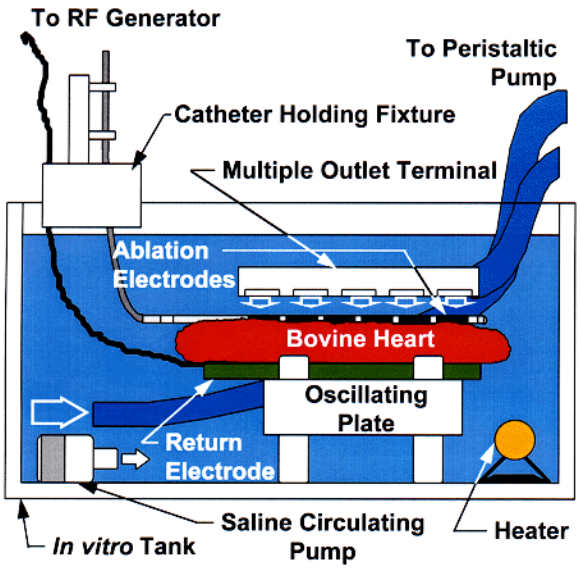

Figure 3. Side view of the *in vitro* apparatus. The tank was filled with 0.45% saline which was heated at 37 °C. A peristaltic pump circulated the saline over the ablation electrodes at a velocity of 12 cm s^{-1}. The oscillating table moved the tissue and the electrodes up and down at a rate of 60 rpm. A holding fixture applied a constant 20 gf to the MEC. The MEC and the return electrode were connected to the RF generator via the APM.

of the heart motion, the oscillating table moved the tissue and the MEC up and down at a rate of 60 excursions per minute. The saline concentration was equal to 0.45%, thus approximating a blood electrical conductivity of ≈150 Ω cm. A heater regulated the saline temperature at 37 °C. The MEC and the return electrode were connected to the APM, as indicated in figure 2.

During the *in vitro* experiments we analysed: (1) the validation of the FE model described in section 2.2; (2) the feasibility of achieving long contiguous lesions without moving the MEC; (3) the lesion dimensions as a function of the number of ablating coil electrodes; (4) the system parameters (i.e. temperature, power and impedance) during simultaneous RF application to multiple coil electrodes. Lesions were created with one up to six coil electrodes at user-defined set temperature points of 60, 70, 80 and 90 °C. The RF generator was operated in a temperature-controlled mode so that the temperatures at all selected coil electrodes were regulated about the set temperature value. Upon completion of the desired lesion set, the tissue was dissected and the lesion dimensions measured. The dissection was first performed longitudinally. Then cross-sectional dissections were performed to analyse tissue beneath coils and intercoil gaps. The lesion dimensions were measured based on the boundaries of tissue discoloration. In a previous study, we have reported that the bovine heart used in our experiments changed colours from red-purple to white-red at an average temperature of 60 °C (Panescu *et al* 1995a). Therefore, the reported *in vitro* lesion dimensions correspond to 60 °C isothermal surfaces. During *in vivo* RF applications, myocytes are rendered non-viable at an average temperature of 50 °C (Nath *et al* 1993). Consequently, on average, our reported *in vitro* lesion dimensions may underestimate *in vivo* dimensions.

2.5. In vivo method

Several studies report on the use of RF ablation to achieve therapeutic lesions for the cure of Afib (Swartz *et al* 1994, Haines and McRury 1995, McRury *et al* 1997, Gupta *et al* 1998). To this date, a commonly accepted therapeutic lesion set has not yet been found. Therefore, we focused our *in vivo* experiments on three of the right-atrial lesion lines that have been mentioned or analysed by most prior studies: (1) posteriorly from the inferior vena cava (IVC) to the superior vena cava (SVC); (2) from the IVC to the tricuspid annulus (TA); and (3) along the right atrial free wall anteriorly descending to the TA from the proximity of the SVC and passing close to the right atrial appendage. Studying only these three lines represents a limitation of this study. Complete treatment of Afib may require lesions at other locations as well. Figure 4 illustrates the approximate location of these three lesion lines within the right atrium. The lesions were studied on a group of eight mongrel canines weighing 25–40 kg. The animals were anaesthetized with Nembutal and ventilation was performed to maintain a blood oxygen concentration above 98%. Heparin dosage of 2000–5000 units was used. To minimize the chances of pulmonary embolus, heparin was administered intravenously. The MEC was placed into the right atrium via an 8F introducer inserted into the femoral vein using the Seldinger technique. Intracardiac electrograms and surface ECGs were monitored. Tissue–electrode contact was confirmed by pacing from the selected coil electrodes and monitoring heart capture. The lesions were performed using the ablation system described in figure 2. The set temperature was 70 °C, the duration of RF application was 60 s and the energy was transmitted to one or two coil electrodes. Because the technology was in the initial phase of the learning curve, we limited the RF application to up to two coil electrodes at a time. We monitored the procedure and fluoroscopy times required to create each of the three lesion types. Up to four weeks after the procedure, the animals were sacrificed and the hearts dissected. Tissue was stained with nitroblue tetrazolium kept at 37 °C (Gottlieb *et al* 1981, Haines 1991). Lesion depth, width and length were measured. Lesions which were transmural, contiguous and extended over

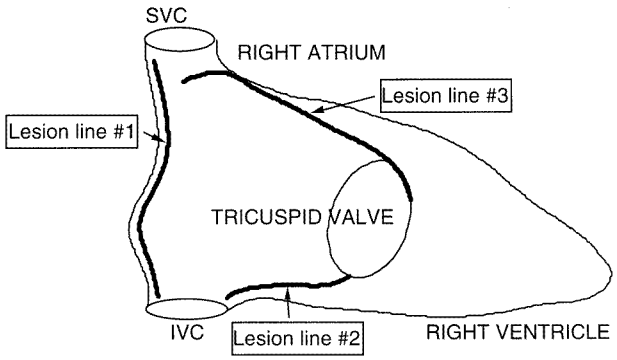

Figure 4. Simplified view of the anatomical locations of the right-atrial lesion lines analysed by the *in vivo* study.

the desired contour without displaying char or desiccation were considered to have increased chances of being therapeutically effective.

3. Results

3.1. Distribution of SAR and current density values

The current densities in figure 5 were computed based on the SAR values averaged over five different type 1 and 2 experiments, respectively, as specified in section 2.1. Because the ends of each coil electrode were covered by a thin layer of electrically insulating UV adhesive, discontinuity in electrical conductivity occurred at coil ends. Consequently, higher current densities were expected at the ends of the coil electrodes. Indeed, as figure 5 indicates, higher current density values were measured at the coil ends during both the one- and two-coil tests. Figure 5(*b*) shows higher current density values at the proximal end of the proximal coil and at the distal end of the distal coil than at the distal end of the proximal coil and at the proximal end of the distal coil respectively. These results were caused by the proximity of the metallic surfaces of the coils. Because in the two-coil experiments the electrodes were connected in parallel, their surfaces were equipotential. Hence it is expected the current density maxima at the inner coil ends be somewhat lower than the current density maxima at the outer coil ends.

3.1.1. Validation of the electrical–thermal FE model. To validate the results of the numerical analyses, comparisons of essential ablation parameters measured using the *in vitro* apparatus and simulated using the one-coil FE model were performed. A total of $N = 3$ experiments were performed for each comparison. Table 2 summarizes the validation results. A maximum relative error of 13.5% was found in mispredicting the necessary RF power to reach a measured average maximum tissue temperature of 91.3 °C. Because the optimal temperature-sensor placement was more affected by the relative distribution of tissue temperatures rather than by the exact power levels, these FE model accuracy levels were considered acceptable.

3.1.2. Results of electrical–thermal FE analyses. Figure 6 presents the temperature distribution resulting from the electrical–thermal FE analysis described in section 2.2. The equivalent total power applied to the one-coil-electrode model was 16 W resulting in a system impedance of $\approx$91 Ω. The maximum temperature reached 82.1 °C and was located in the tissue

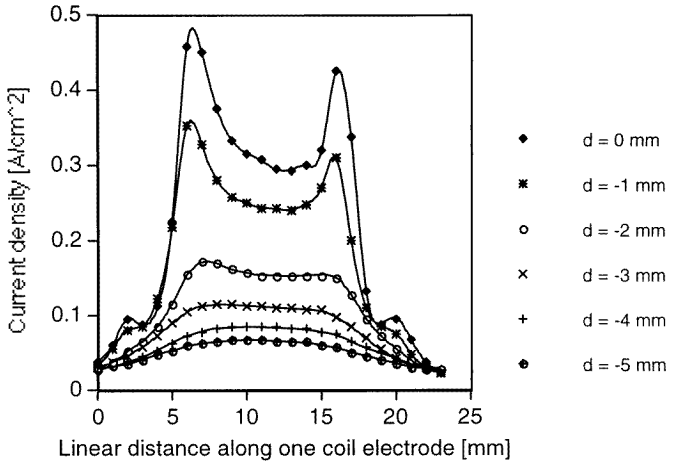

(a)

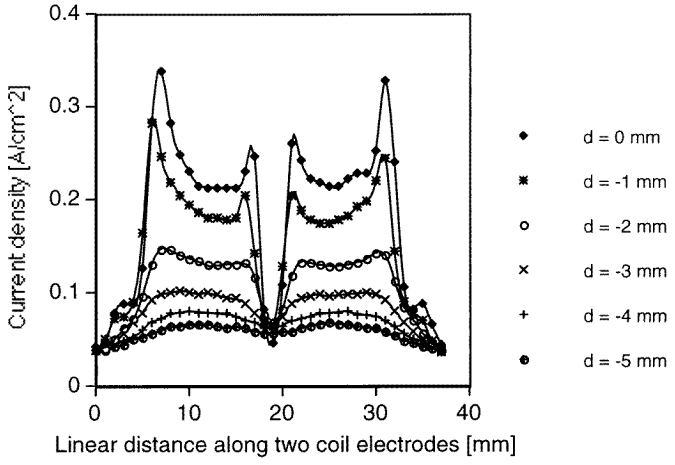

(b)

Figure 5. (*a*) Current density profiles at various distances under one coil electrode. Maximum standard deviation 0.051 A cm^{-2}. (*b*) Current density profiles at various distances under two coil electrodes. Maximum standard deviation 0.023 A cm^{-2}. The electrodes were placed in a 0.15% saline tank and 20 W of RF power were applied with respect to a return electrode. The maximum current density values were reached at the coil ends.

region ≈0.3 mm beneath the coil ends. The 50 °C isothermal surface extended vertically ≈6 mm deep into the tissue and horizontally ≈2 mm beyond each end of the coil. Most of the blood volume next to the coil reached temperatures below 60 °C. The simulations also estimate that blood flowing more than 2 mm away from the coil may heat to less than 50 °C. The blood temperature reached values between 70 and 75 °C just above the layers of UV adhesive covering the ends of the coil. The presence of the UV adhesive reduces the local current density values and thereby limits abrupt rises in local temperatures (Panescu *et al* 1995a). To minimize chances of charring and coagulation, it is important to control the applied RF power such that the resulting edge temperatures are less than 100 °C (Cosman and Rittman 1995).

Table 2. Validation of the one-coil 3D FE model. The measured ($N = 3$) applied voltage (V), current (I), power (P), impedance (Z) and the resulting temperature at the sensor location (T_{CE}), maximum tissue temperature (T_t), lesion length (L) and depth (D) are compared with the corresponding results of the FE analyses (based on 60 °C contour).

	V (V)	I (A)	P (W)	Z (Ω)	T_{CE} (°C)	T_t (°C)	L (mm)	D (mm)
Measured	38.6 ± 0.88	0.4 ± 0.01	14.1 ± 0.05	94 ± 4.5	70 ± 5.7	91.3 ± 4.3	14.8 ± 0.3	4.8 ± 0.1
Simulated	38.22	0.42	16	91	68	82.1	15.4	4.4
Error (%)	−1	5	13.5	−3.2	−2.8	−9.6	4	−8.3

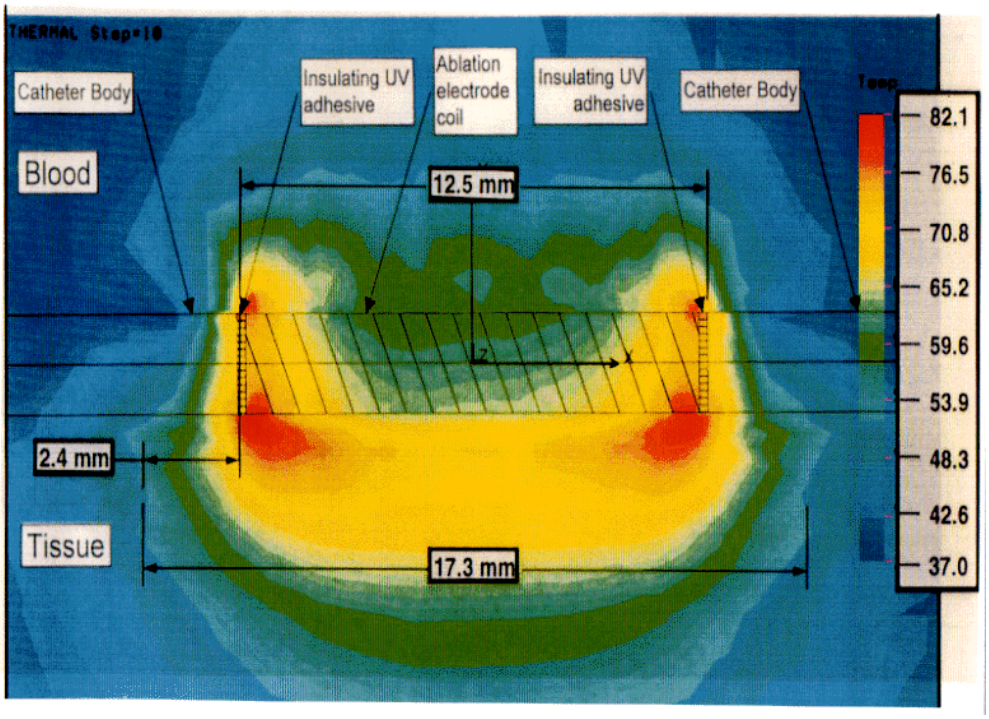

Figure 6. Temperature distribution resulting from the FE simulations of RF ablation with one 12.5 mm long coil electrode. The ablation duration was 120 s and the applied power was 16 W. The equivalent system impedance was ≈91 Ω. The maximum temperature was reached in the tissue region ≈0.3 mm beneath the ends of the coil.

The temperature values within the catheter body dropped to ≈37 °C at distances of more than 3 mm from the coil ends. This ensured that the cold junction was not heated by the most proximal coil electrode. The distance between the cold junction ring and the most proximal coil electrode was ≈5 cm. The results of the FE analyses compare well with results published by McRury *et al* (1997).

3.2. Multielectrode catheter construction details

Both the SAR measurements and the FE analyses indicated that more heating occurred at the coil ends than at its centre. To avoid undesired effects of tissue and blood overheating at temperatures approaching 100 °C it was important to control the temperatures at the end regions. For this reason, we decided to place a temperature sensor interior to each end of

the coil electrodes. The sensors were in thermal contact with the metal of the coil and placed in diametrically opposite positions. Thus in most situations one sensor was facing the tissue and the other the blood. As presented in section 2.3, the APM assigned T_{CE} equal to the higher of these two values. The RF generator controlled the applied power such that all selected T_{CE} values were within a 5 °C interval about the user-defined set temperature. Consequently, temperatures at any of the coil ends were controlled within a safe range below 100 °C.

The length of the coil electrode was chosen equal to 12.5 mm. Ideally, the coil electrode would be as long as possible. However, practical requirements make coils with excessive length unfeasible. Also, due to resistive losses along the coil, heating may not occur at the ends of very long coils. The length chosen represented a compromise of all these requirements.

One of the design requirements was that the MEC be capable of generating contiguous lesions. Obviously, if the intercoil distance were too large contiguous lesions would not be created. The FE analyses indicated that heating above 50 °C may occur up to 2 mm beyond selected coil ends. Hence, we estimated that due to additive heating effects contiguous lesions would be achievable with up to 4 mm intercoil distances. Beyond this limit, the 50 °C isothermal boundaries at adjacent coils might not abut, thereby leaving gaps of viable tissue within the lesion profile. Given that the SAR measurements indicated lower current density maxima at the inner ends of adjacent simultaneously powered coils, we have conservatively chosen an intercoil distance of 2 mm.

Table 3. Comparison of mechanical parameters of MECs with different spacing between coil windings.

Parameter	0 mm spacing	0.17 mm spacing
Curvature (mm)	28.2	19.6
Coil-to-coil deflection angle (deg)	31	14

It was also important to determine whether coils should have any separation between windings. Table 3 presents a comparison of mechanical parameters of two MECs with 12.5 mm long coils. One of them had 0 mm and the other 0.17 mm spacing between coil windings. Note that the MEC with spread windings achieved a smaller curvature and a lower coil-to-coil deflection angle. The coil-to-coil deflection angle was measured as the angle between lines tangent to adjacent coil profiles. For example, when the MEC is in straight position this angle equals zero. At maximum steering, this angle is smaller for more flexible coils. If the coils were rigid, thus forcing the catheter tubing to kink, this angle would have been wider. A smaller curvature provides improved catheter manoeuvrability, while a smaller coil-to-coil deflection angle results in a smoother catheter profile and improves the tissue–electrode contact.

3.3. Results of in vitro experiments

During RF applications with six coil electrodes the power required to reach any of the tested set temperatures exceeded the generator upper limit of 150 W. For this reason, all six-coil *in vitro* lesions were discarded from these analyses. All lesions created at set temperatures of 60 °C were not contiguous, gaps in tissue discoloration profiles being visible at the intercoil spaces. As mentioned above, tissue discoloration occurred at ≈60 °C. Therefore, the temperatures at the intercoil spaces, which were below the 60 °C set value, did not cause tissue discoloration. The result was a discontinuous lesion aspect. At set temperatures of 70 °C, 85% of the lesions were contiguous. All lesions created at set temperatures of 80 and 90 °C were contiguous. All

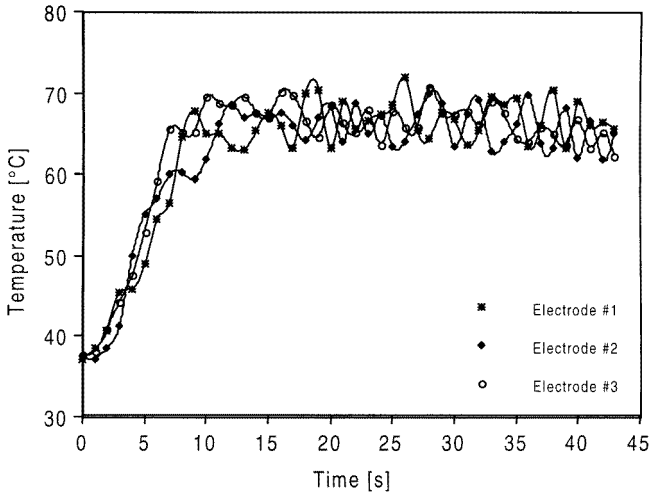

(a)

(b)

Figure 7. (*a*) Temperature recordings (T_{CE}) at three coil electrodes during simultaneous RF application. (*b*) Cross section of *in vitro* lesion obtained during ablation with three coil electrodes. The set temperature was 70 °C and the lesion was contiguous.

contiguous lesions were generated without catheter repositioning or movement. Charring was not present in any of the analysed lesions and no sudden impedance rises occurred. The average lesion depth increased with set temperature. The average depth was 2.6 mm at 60 °C ($N = 38$), 3.9 mm at 70 °C ($N = 39$), 4.3 mm at 80 °C ($N = 39$) and 4.5 mm at 90 °C ($N = 39$). As a reminder, these values refer to the depth of the 60 °C isothermal surface, marking the tissue discoloration border. Table 4 presents the dependence of lesion length, power and system impedance on the number of coil electrodes to which RF energy was simultaneously applied. The lesion length increased almost linearly with the number

Table 4. Dependence of *in vitro* lesion length, RF power and system impedance on the number of ablating coil electrodes. The set temperature was 70 °C and the flow velocity was ≈12 cm s^{-1}.

	Number of electrodes				
Parameter	1 ($N = 9$)	2 ($N = 9$)	3 ($N = 8$)	4 ($N = 7$)	5 ($N = 6$)
Lesion length (mm)	16.7 ± 1.7	32.8 ± 2.1	47.8 ± 4.1	64.7 ± 4.2	80.1 ± 6.2
Power (W)	17.5 ± 5.7	42.9 ± 9.3	74.9 ± 13.6	96.4 ± 15.8	108.3 ± 13.9
Impedance (Ω)	94.1 ± 2.2	68 ± 4.8	51.7 ± 4.6	48.7 ± 2.9	45.5 ± 2.7

of electrodes (the approximation $y = 0.8 + 15.9x$ yields $r = 0.99$). Lesion length varied insignificantly with the set temperature. Power requirements to reach a set temperature of 70 °C were larger as more electrodes were driven by the RF generator. The system impedance decreased as more electrodes were connected in the ablation circuit and reached a low of 45.5 Ω with five coil electrodes in the circuit. With only one coil electrode in the circuit, the average measured impedance was 94.1 Ω. Comparatively, the impedance resulting from the FE simulations was 91 Ω. Figure 7(*a*) shows the measured T_{CE} when RF power was simultaneously applied to three coil electrodes at a set temperature of 70 °C. The average temperature at each electrode was regulated within a 5 °C interval about the set temperature. Figure 7(*b*) shows a cross-section through the lesion obtained during the RF application recorded in figure 7(*a*). Lesion thinning is observed at the distal end of the catheter due to its proximity to the flow source.

3.4. Results of in vivo experiments

The total procedure and fluoroscopy times, averaged over all eight experiments, were 83.4 and 5.9 min respectively. Table 5 presents these times and the average lesion width and length for each of the three lesions analysed. No sudden impedance rises occurred and 75% of the lesions were contiguous. Slight coagulation was found at the ends of 9% of the total number of coils which delivered RF energy. From the set of contiguous lesions, 90% were potentially therapeutic as they were transmural and extended over the entire desired contour, as specified in section 2.5. Figure 8(*a*) represents the temperature recordings during one of the two-coil *in vivo* RF ablations. Figure 8(*b*) shows two of the *in vivo* lesions at one-week follow-up. The lesion marked A was along line #3 and the lesion marked B was along line #1, as specified in section 2.5. Table 6 shows the power required to reach set temperature and the system

Table 5. Lesion dimensions, procedure and fluoroscopy times for the three types of atrial lesions.

Parameter	Line #1	Line #2	Line #3
Procedure time (min)	42.9 ± 18	17.9 ± 5.5	12.4 ± 3.7
Fluoroscopy time (min)	4.6 ± 2.5	1.1 ± 0.6	0.7 ± 0.7
Lesion width (mm)	7.1 ± 1.2	5.9 ± 0.7	8.5 ± 1.9
Lesion length (mm)	59.2 ± 11.7	17.6 ± 6.1	47.6 ± 15.3

Table 6. Power and impedance during *in vivo* RF applications.

Parameter	One coil electrode	Two coil electrodes
Power (W)	39 ± 17	87 ± 12
Impedance (Ω)	105 ± 16	75 ± 12

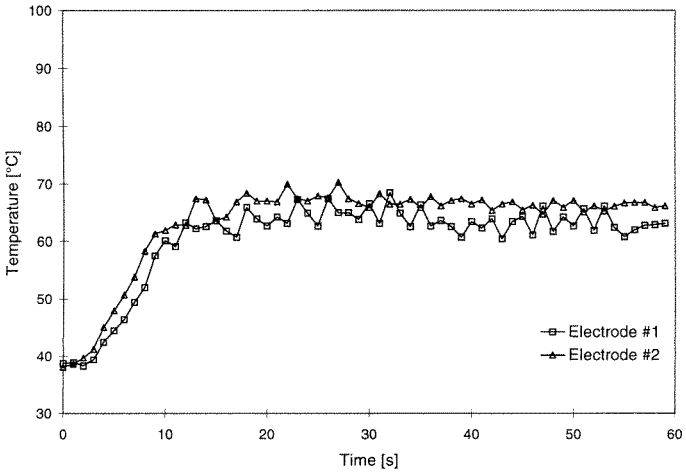

(a)

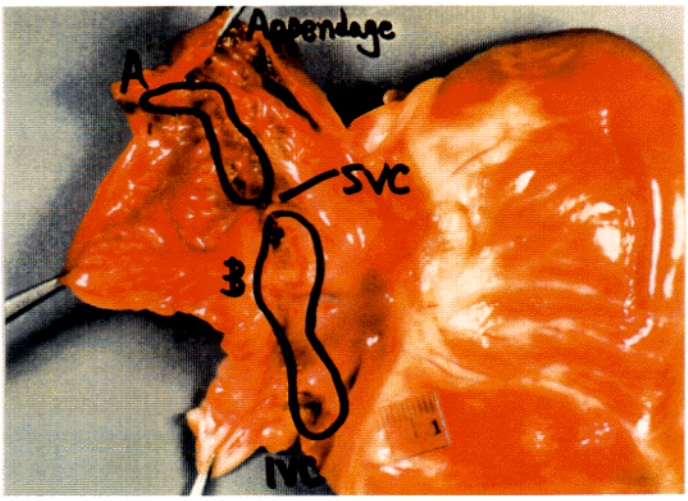

(b)

Figure 8. (*a*) Temperature recordings (T_{CE}) at two coil electrodes during simultaneous *in vivo* RF application. The set temperature was 70 °C. (*b*) In vivo atrial lesions obtained with the MEC. Two of the three lesion lines specified in the text are shown. The lesion marked as A was along line #3. The lesion marked as B was along line #1.

impedance during *in vivo* ablations with one and two coil electrodes. The average impedance values were consistent with numbers reported by the FE analyses and the *in vitro* studies. The average power levels were significantly higher than what was expected based on FE and *in vitro* analyses. Possible explanations for this difference are worse electrical tissue–electrode contact during the *in vivo* ablations and stronger convective cooling effects of the turbulent and pulsatile blood flow.

4. Discussion

The SAR measurements indicated higher current densities at the ends of coils. This was an expected result given the discontinuity in local electrical conductivity at the junction between the metallic coil and the UV adhesive. The FE analyses predicted higher temperature values at the coil ends, consistent with the SAR results. Therefore, we decided to place two temperature sensors at the ends of each coil electrode. The sensors were placed at diametrically opposite locations, such that, in most cases, one faced the tissue and the other the blood. Temperatures from all selected sensors were analysed by the APM. Each selected coil was assigned a temperature value equal to the higher of the two sensor readings. This feature of the system allowed both tissue and blood temperatures to be controlled within a safe range below 100 °C, and, thereby, to minimize incidences of charring or coagulation. Although *in vivo* ablation power levels in excess of 100 W were reached, no sudden impedance rise occurred and no char was found by post-ablation electrode inspection. Another goal of our system design was to provide features needed for generating contiguous lesions. The FE analyses predicted that the 50 °C isothermal surface extends approximately 2 mm beyond the coil ends during single-coil ablation. This result indicated that an electrode placement with 2 mm intercoil spacing can benefit from the additive heating effects occurring at the gaps between coils. Higher coil-end current densities, as measured by the SAR technique, also contribute to additive heat generation at the intercoil spaces. As a result of this electrode placement, all *in vitro* lesions created at set temperatures higher than 70 °C were contiguous. Also, 75% of the *in vivo* RF applications resulted in complete lesions at the gaps between coils. It was also required to provide the catheter with efficient manoeuvrability such that it could be steered safely at the therapeutic location and that it had to conform smoothly to the irregular shapes of the atrial wall. We found that having the coil windings spaced apart improved the MEC curvature and coil-to-coil deflection angle. In return, these improvements resulted in successful, rapid and safe catheter positioning at the locations corresponding to the analysed lesion types. At post-ablation lesion inspection, 90% of the *in vivo* contiguous lesions were considered potentially therapeutic, as they were transmural and expanded along the intended contour. All these features, in conjunction with the temperature control provided by the APM, resulted in reduced procedure and fluoroscopy time. We conclude that the system can safely perform long and contiguous lesions in canine right atria.

The technological problem of providing appropriate medical equipment for the cure of Afib by RF ablation is far from being completely solved. We believe that further improvements can be achieved in the design of the steering platform, such that better conformance to the atrial wall and superior tissue–electrode contact are offered. As a limitation, this study did not address some catheter features which are desired for RF ablations in the left atrium. For example, recent reports have indicated that contiguous lesions which isolate the pulmonary veins or point lesions in the pulmonary veins may be necessary for successfully treating Afib (Ernst *et al* 1998, Wharton *et al* 1998). As a future goal, we consider improved combinations of sheath, introducers and multielectrode catheters which would be suitable for a transeptal approach to left atrial RF ablation.

References

Allessie M A, Bonke F I and Kirchhof C J 1990 Atrial reentry *Cardiac Electrophysiology* ed M R Rosen, M J Janse and A L Wit (Mount Kisco, NY: Futura)

ASM International 1992 *ASM Handbook* 10th edn (Materials Park, OH: ASM International)

Cosman E R and Rittman W J 1995 Physical aspects of radiofrequency energy applications *Radiofrequency Catheter*

Ablation of Cardiac Arrhythmias. Basic Concepts and Clinical Applications ed S K S Huang (Armonk, NY: Futura) pp 13–39

Cox J L, Schuessler R B and Boineau J P 1991b The surgical treatment of atrial fibrillation: summary of current concepts of mechanism of atrial flutter and atrial fibrillation *J. Thorac. Cardiovasc. Surg.* **101** 402–5

Cox J L, Schuessler R B, D'Agostino H J, Stone C M, Chang B C, Cain M E, Corr P B and Boineau J P 1991a The surgical treatment of atrial fibrillation: development of a definitive surgical procedure *J. Thorac. Cardiovasc. Surg.* **101** 569–83

Ernst S, Ouyang F, Volkmer M, Hebe J, Antz M, Cappato R, Schloter M and Kuck K-H 1998 Clinical follow-up after primary catheter ablation of atrial fibrillation using the CARTO system *AHA Abstracts Circ.* **98** I–180

Gottlieb G J, Kubo S H, Alonso D R 1981 Ultrastructural characterization of the border zone surrounding early myocardial infarcts in dogs *J. Pathol.* **103** 292–303

Gupta G, Millard S, Urbonas A, Helms R and Avitall B 1998 The creation of linear lesions to ablate atrial fibrillation: 12 mm coil electrodes vs 4 mm ring electrodes *NASPE Abstracts PACE* **21** 804

Haines D E 1991 Determinants of lesion size during radiofrequency catheter ablation: the role of electrode-tissue contact pressure and duration of energy delivery *J. Cardiovasc. Electrophys.* **2** 509–15

Haines D E and McRury I A 1995 Primary atrial fibrillation ablation in a chronic atrial fibrillation model *AHA Abstracts Circ.* **92** I–265

Haissaguerre M, Marcus F I and Fischer B 1994 Radiofrequency catheter ablation in unusual mechanism of atrial fibrillation: report of three cases *J. Cardiovasc. Electrophys.* **5** 743–51

IEEE Standards Coordinating Committee 28 1992 *IEEE Std C95.3-1991: IEEE Recommended Practice for the Measurement of Potentially Hazardous Electromagnetic Fields–RF and Microwave* (New York: IEEE)

Incropera F P and DeWitt D P 1985 *Fundamentals of Heat and Mass Transfer* 2nd edn (New York: Wiley)

Jaïs P, Haïssaguerre M and Shah D 1996 Characteristics of focal atrial fibrillation *NASPE Abstracts PACE* **19** 650

McRury I A, Panescu D, Mitchell M A and Haines D E 1997 Nonuniform heating during radiofrequency catheter ablation with long electrodes *Circulation* **96** 4057–64

Mirotznik M S, Cheever E and Foster K R 1996 High resolution measurements of specific absorption rate of small antennas in tissue *IEEE Trans. Instrum. Meas.* **45** 754–6

Nath S, Lynch C, Whayne J G and Haines D E 1993 Cellular electrophysiologic effects of hyperthermia on isolated guinea pig papillary muscle: implications for catheter ablation *Circulation* **88** 1826–31

Panescu D 1997 Intraventricular electrogram mapping and radiofrequency ablation for ventricular tachycardia *Physiol. Meas.* **18** 1–38

Panescu D, Fleischman S D, Whayne J G and Swanson D K 1995b Contiguous lesions by radiofrequency multielectrode ablation *Proc 17th Ann. Int. Conf. IEEE Engineering in Medicine and Biology Society (Montreal, 1995)* (Piscataway, NJ: IEEE) pp 275–6

Panescu D, Whayne J G, Fleischman S D, Mirotznik M S, Swanson D K and Webster J G 1995a Three-dimensional finite element analysis of current density and temperature distributions during radio-frequency ablation *IEEE Trans. Biomed. Eng.* **42** 879–90

Rabbat A 1990 Tissue resistivity *Electrical Impedance Tomography* ed J G Webster (Bristol: Adam Hilger)

Roberts S A, Diaz C, Nolan P E, Salemo D M and Stapczynski J S 1993 Effectiveness and costs of digoxin treatment for atrial fibrillation and flutter *Am. J. Cardiol.* **72** 567–73

Shitzer A and Eberhart R C 1985 *Heat Transfer in Medicine and Biology* (New York: Plenum)

Swartz J F, Pellersels G and Silvers J 1994 A catheter-based curative approach to atrial fibrillation in humans *AHA Abstracts Circ.* **90** I–335

Tong P and Rossettos J N 1977 *Finite Element Method* (Cambridge, MA: MIT)

Wharton M J, Vergara I, Shander G, Bahnson T D, Sorrentino R A and Greenfield R A 1998 Identification and ablation of focal mechanisms of atrial fibrillation *AHA Abstracts Circ.* **98** I–18

Wolf P A, Abbott R D and Kannel W B 1991 Atrial fibrillation as an independent risk factor for stroke: the Framingham study *Stroke* **22** 983–8